

Supplementary Information for

Precisely Tuning Band Gaps of Graphene/h-BN

Lateral Heterostructures Toward Enhanced

Photocatalytic Hydrogen Evolution

Huizhong Ma,^a Yulong Wang,^a Lingling Sun,^a Chunyan Wang,^a Liwei Wang,^a Zhuang Ma,^a Honglei Yuan,^{*a} Jin Feng^{*b}

^a*School of Physics and Telecommunication Engineering, Zhoukou Normal University, Zhoukou 466001, China*

^b*Key Laboratory of Life-Organic Analysis of Shandong Province, School of Chemistry and Chemical Engineering, Qufu Normal University, Qufu 273100, China*

**E-mail Addresses: fengjinzuibang@163.com (J. Feng), yhl@zknv.edu.cn (H. Yuan).*

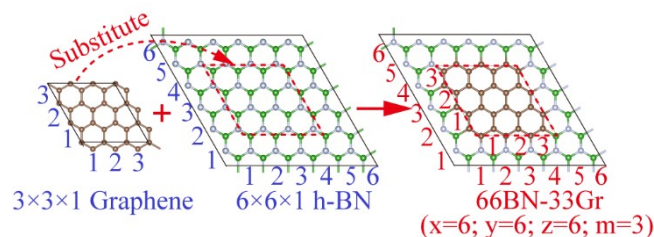


Figure S1. The conceptual framework and nomenclature conventions for the formation of 66BN-33Gr.

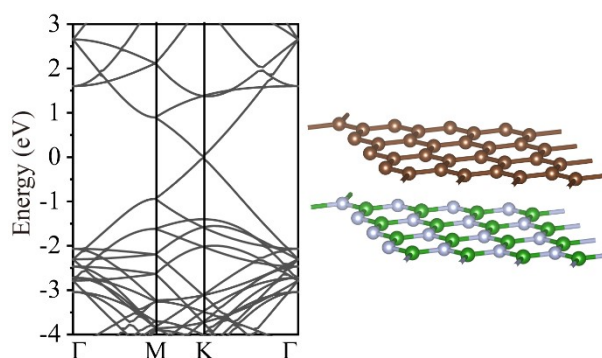


Figure S2. DFT-PBE calculated band structure (left panel) and geometric configuration (right panel) of vertically stacked graphene/h-BN heterostructure.

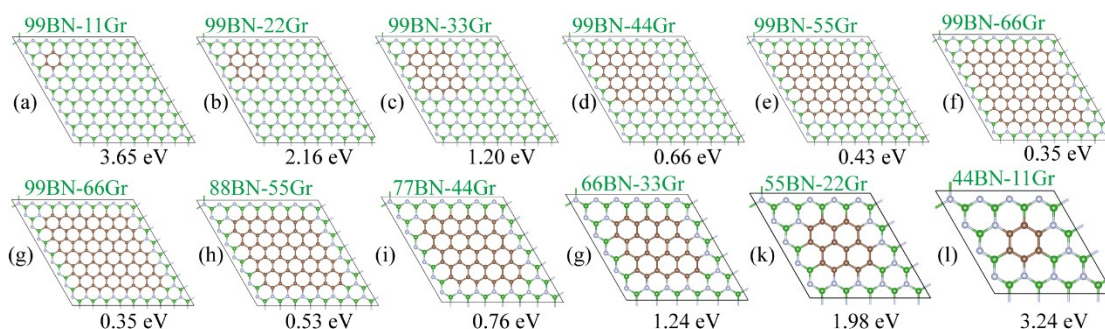


Figure S3. Structural configurations, nomenclature, and band gap values of graphene/h-BN lateral heterostructures with systematically varied domain dimensions. These configurations correspond directly to those presented in Fig. 1a of the main text.

	99BN-22Gr	99BN-14Gr
Carbon concentration (%)	9.88	11.11
Band gap (eV)	2.16	1.54

Figure S4. Geometric structures, carbon concentrations, and band gaps of 99BN-22Gr and 99BN-14Gr.

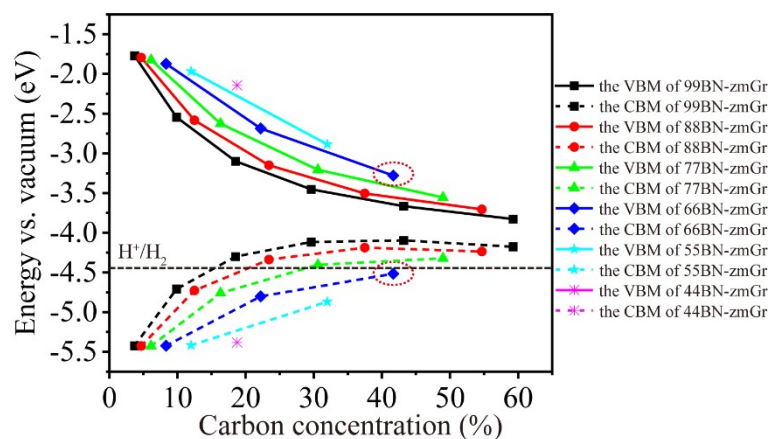


Figure S5. Evolution of valence band maximum (VBM) and conduction band minimum (CBM) energy levels in xyBN-zmGr as a function of carbon concentration, with vacuum level set to 0 eV. The energy levels of 66BN-33Gr are highlighted by a red dashed circle. The hydrogen evolution reaction (HER) energy level is indicated by black dashed lines.

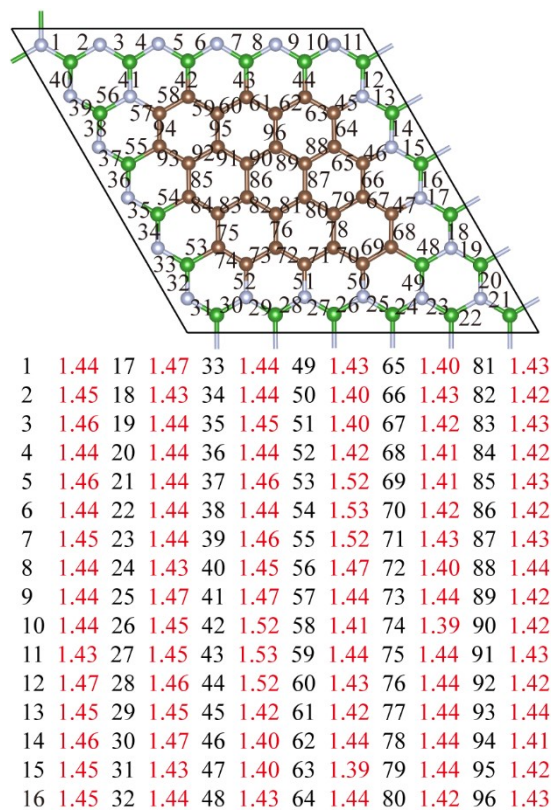


Figure S6. Structural details of 66BN-33Gr with numbered bonds (1-96) and their corresponding lengths (red values in Å).

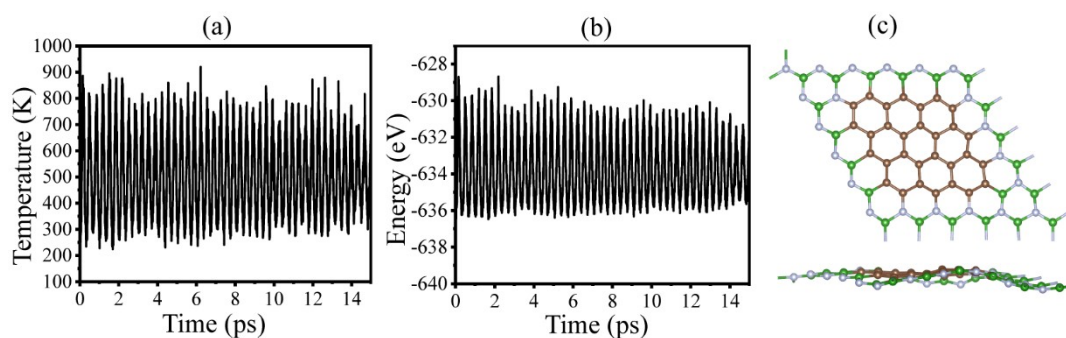


Figure S7. AIMD simulation results for 66BN-33Gr heterostructure at 500 K. (a) Temperature evolution profile during the simulation timeframe. (b) Corresponding total energy fluctuations of the system. (c) Structural snapshot at 15 ps, showing both top and side views of the thermally equilibrated configuration.

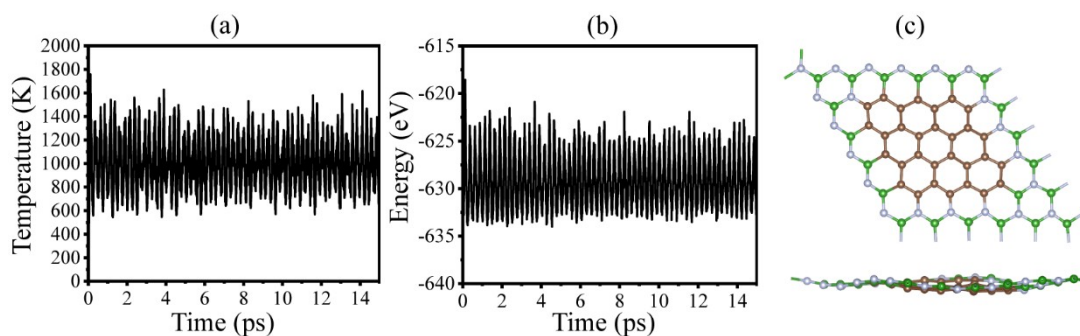


Figure S8. AIMD simulation results for 66BN-33Gr heterostructure at 1000 K. (a) Temperature evolution profile during the simulation timeframe. (b) Corresponding total energy fluctuations of the system. (c) Structural snapshot at 15 ps, showing both top and side views of the thermally equilibrated configuration.

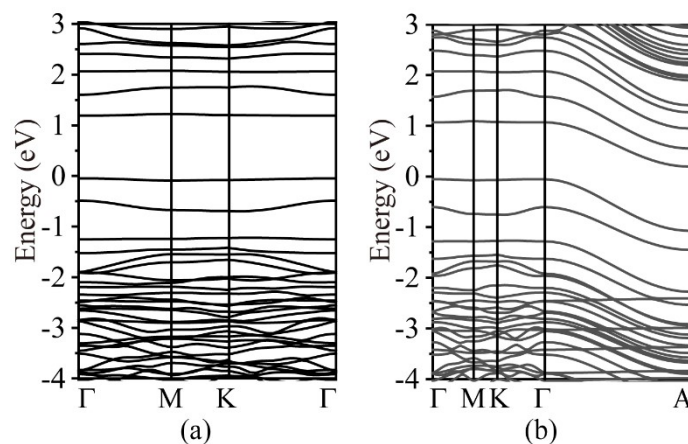


Figure S9. DFT-PBE calculated electronic band structures of (a) monolayer and (b) AA-stacked bulk 66BN-33Gr.

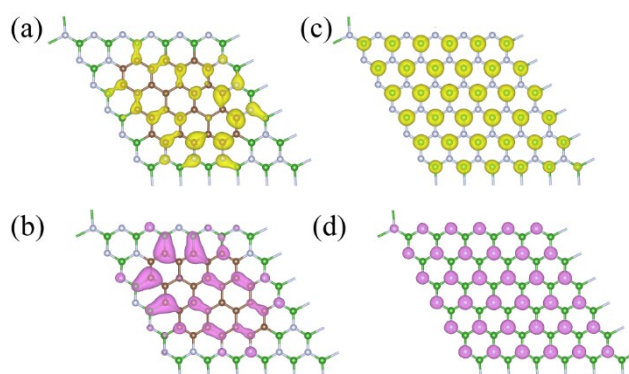


Figure S10. Spatial distributions of photogenerated electrons (yellow isosurfaces) and holes (magenta isosurfaces) for the lowest excited states of (a,b) 66BN-33Gr and (c,d) h-BN.

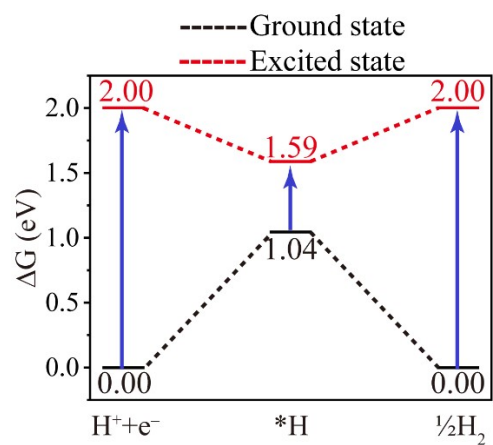


Figure S11. Free energy diagrams of HER at site C16 for both ground state (black line) and excited state (red line).